TURBULENT FLUXES IN COMPLEX TERRAIN AND THE EFFECTS OF STATIC STABILITY

Nigel Wood
The Meteorological Office
Bracknell,U.K.

1 INTRODUCTION

Studies of flow over hills and mountains to date largely fall into one of two categories: *neutrally-stratified turbulent* flow over hills embedded within the boundary layer; and *stably-stratified inviscid* flow over hills or mountains penetrating the boundary layer. The study of non-neutrally stratified but turbulent flow over hills has received relatively little attention.

Chimonas and Nappo (1989) and Grisogono (1994) attempted to make some allowance for the gross effects of the boundary layer on the structure and effects of gravity waves. Also Shutts and Broad (1993) and Ólafsson and Bougeault (1997) recognised the importance of the no-slip surface boundary condition in correctly determining the wave field in stable flow over mountain ranges. However, with these notable exceptions most of the attention this subject has received has originated from the boundary-layer community.

On the theoretical side Hunt *et al.* (1988b) extended the linear analysis of neutral flow over low sloped hills of Hunt *et al.* (1988a) to stably-stratified flow and thus described the broad features of the flow. Then Belcher and Wood (1996) extended the linear, neutral calculation of the pressure force induced by turbulent flow over hills (Belcher *et al.* 1993) to the weakly stratified case and compared their results with non-linear numerical simulations.

Observations have largely focussed on the mean flow structure, primarily the flow at the crest. For example, Bradley (1983), Frank *et al.* (1993) and Coppin *et al.* (1994) have all made measurements of the flow speed-up at the crest of hills in stable situations. Stromberg *et al.* (1989) also measured the flow speed-up at the crest of a hill in stable conditions but their main interest was in measurements of the lee wave structure which they made using a sailplane. Mason (1987) made detailed measurements of the vertical profiles and near surface flow in a quasi-two-dimensional ridge-valley system. The measurements were made during the transition from daytime unstable to nocturnal stable conditions and were simulated using a two-dimensional numerical model. In this study the slopes of the hill were large enough to induce mean flow separation.

Numerical modelling studies of non-neutrally stratified, turbulent flow over hills are, if anything,

fewer in number than the theoretical and observational studies. Schumann (1990), Krettenauer and Schumann (1992) and Dörnbrack and Schumann (1993) have performed large-eddy simulations of unstably stratified flow over two-dimensional hills and slopes. On the stable side, in addition to the numerical modelling already alluded to, Weng *et al.* (1997) extended a linear numerical model of neutral flow over hills to allow for the effects of stability. They showed the variation of the pressure drag with Froude number also made comparisons with inviscid model results. Zhou *et al.* (1995) used a similar linear model to study the influence of the boundary layer on gravity waves and, for their cases, showed that the boundary layer does influence the wave field primarily through the influence of wind shear. Inglis *et al.* (1995) used a numerical implementation of the theoretical ideas of Hunt *et al.* (1988) and obtained reasonable agreement with observations of the mean flow structure over a complex but reasonably isolated piece of terrain. All of these stably-stratified numerical studies have been limited to low slopes, either due to the limitations of the models or by choice (Belcher and Wood 1996) in order to compare with linear theory.

In contrast to these relatively recent and small number of studies of weak to moderate stable flow over hills there is also an extensive literature on the very stable flows associated with drainage currents or katabatic flows (Price (1995) gives a comprehensive review). However, the interest of this study is with those cases where, whilst the flow is non-neutral, there is sufficient wind for the associated momentum drag to be an important factor.

Even with the collected knowledge of the above studies there is still very little understanding of the effects of stable stratification. Hunt and Richards (1984) showed that the effects of stratification can be considered as comprising two effects: one is the kinematic effect of changes in the undisturbed flow profiles; the other is the dynamic effect of buoyancy forces. This was also demonstrated by Belcher and Wood (1996) in their analysis of the pressure force in stable situations. One thing that seems clear is that stable stratification increases the flow speed-up at the crest. From Coppin *et al.*'s experimental results and Hunt *et al.*'s theoretical work it seems reasonably well established that the flow speed-up is primarily due to the increased shear in the background, undisturbed flow, i.e. the kinematic effect. This increase in shear seems also to be a critical factor in determining the pressure force on the hill (Belcher and Wood). However, predicting this increase in shear requires understanding of the effect of stratification on the relevant depth scales of the flow yet there is debate in the literature over whether stratification actually increases or decreases the middle-layer depth. We are still some way then from making estimates of their actual value with any great certainty! Even less clear is what the equivalent effect on the decrease in the wind speed in the valley is and what the resulting impact on flow separation is (Hunt and Richards 1984; Mason 1987).

Some of the reasons for this lack of understanding are clear. It is quite natural to start with the

easiest simplification. For the boundary-layer community this is neutral stratification whilst for the gravity-wave community it is inviscid flow. As understanding of these problems grows only then does attention turn to the harder problems. And stable stratification does add considerable difficulty to the problem of viscous flow over hills. The sensitivity of such flows to even small perturbations and small slopes is well documented (Mahrt 1982; Derbyshire and Wood 1994). This tends to make any study quite specific to the particular problem in hand. This is only exacerbated by the increase in defining parameters. For example, in addition to the defining parameters for boundary-layer flow, neutral flow over hills may in general terms be described by the following parameters: $(h/\lambda; Z_0/\lambda)$ where h is the hill height, λ a measure of its horizontal extent and Z_0 the surface roughness length. For stably stratified flows the following parameters must be added: F_λ and Z_i/λ where F_λ is a relevant Froude number and Z_i is the boundary-layer depth. Also three-dimensional effects, characterised by the aspect ratio λ_x/λ_y, are likely to become more critical than in the neutral case.

Added to these problems is the practical issue of making representative turbulence measurements in stable conditions (e.g. Derbyshire 1995). The background conditions also tend to vary more rapidly in such conditions (e.g. Caughey *et al.* 1979) making interpretation of the data difficult (the nocturnal boundary layer tends to continue to evolve throughout the night). Again this tends to make measurements more site specific, making general conclusions harder to draw.

In this paper it is hoped to identify some key issues, highlight areas of sensitivity of stable flow over hills and give some ideas on the way forward. Here the interest is primarily in understanding the overall effects that the interaction of stable-stratification and flow over hills has on the boundary layer with a view to parametrizing such effects in numerical weather prediction models and general circulation models. Apart from Mason (1987) most of the work has so far focussed on low sloped hills for which linear analysis might be applicable. However, because of the much larger flow perturbations found at the crest in stable flows, the range of validity of the linear analysis (which requires the perturbations to be small) is smaller than for the neutral case. It is therefore important to consider what effect larger sloped hills have on the flow structure.

Because of the representivity problems discussed above it is important to cover as wide a part of the parameter space as possible. However, it is hoped that by initially focussing on a particular, idealised case, a luxury afforded by numerical models, and by tying the results to theoretical ideas wherever possible then analysis of a future, more systematic study will be more tractable than otherwise. Thus here results are presented from one particular numerical simulation of stably-stratified flow over a hill.

2 A NUMERICAL CASE STUDY

The primary interest of this study is the impact that a steep hill has on moderately stable flow. As the basis for the case study the parameters of one of the simulations from Series A of Belcher and Wood (1996) is chosen but with the hill height increased. In this way the influence of non-linear, slope dependent processes are highlighted. Whilst, in contrast to the not dissimilar simulation of Mason (1987), it is not intended to particularly simulate a real case, the basic geometry of the hill is chosen to approximately match that of Llanthony (Grant and Mason 1990) in order to be able to qualitatively compare the simulated flow structure with recent measurements of flow in the valley of Llanthony made in stable nocturnal conditions (Holden 1998). A summary of the relevant parameters of the simulation is given in Table 1.

Table 1. CONFIGURATION OF THE NUMERICAL MODEL.

Non-linear solution to the Boussinesq approximation of the Navier-Stokes equations.	
Advection scheme for U,V,W:	2^{nd} order accurate, Piacsek and Williams (1970)
Advection scheme for T and E:	ULTIMATE QUICKEST (Leonard *et al.* 1993)
$1\frac{1}{2}$ order turbulence closure with maximum mixing length $L_0 = 100$m.	
Domain size (width × height):	2000m × 3000m
Vertical grid:	80 points; smallest grid spacing = 2m with lowest level at 1.0m; largest grid spacing = 45m.
Horizontal grid:	20 evenly spaced points.
Hill:	grown from flat to $h = 300$m in 4000 timesteps; 2-D cos squared shape
Surface boundary conditions:	prescribed buoyancy flux = $0.0005\text{m}^2\text{s}^{-3}$; no-slip, logarithmic profile to 1.0m; prescribed surface stress energy ratio = 0.357.
Top of domain boundary conditions:	zero scalar flux; zero stress; zero energy.
Timestep:	recalculated every 10 steps; typically $\Delta t = 6 \times 10^{-3}$s.
Roughness lengths:	$Z_{0m} = Z_{0t} = 0.1$m.
Prandtl number:	$P_r = 1.0$.
Stability functions:	$\alpha_{mo} = \beta_{mo} = 1/0.33$

Whilst it is desirable to match the simulations of Belcher and Wood as closely as possible to allow comparison with results at low slopes, it was found that a reasonably steady initial state is obtained by running the one-dimensional simulation of Belcher and Wood on for a further 11000s. Figure 1 shows the profile of speed used by Belcher and Wood, that used for this simulation (i.e. after 30000s

of simulation time) and that after a total of 50000s simulated time. Extending the one-dimensional simulation in this way does change the initial value of the Monin-Obukhov length, L_{mo}, and hence the value of $1/kL_{mo}$ and so the low slope hill simulations of Series A were repeated and very good agreement with the trend of the values of α from the original simulations was found.

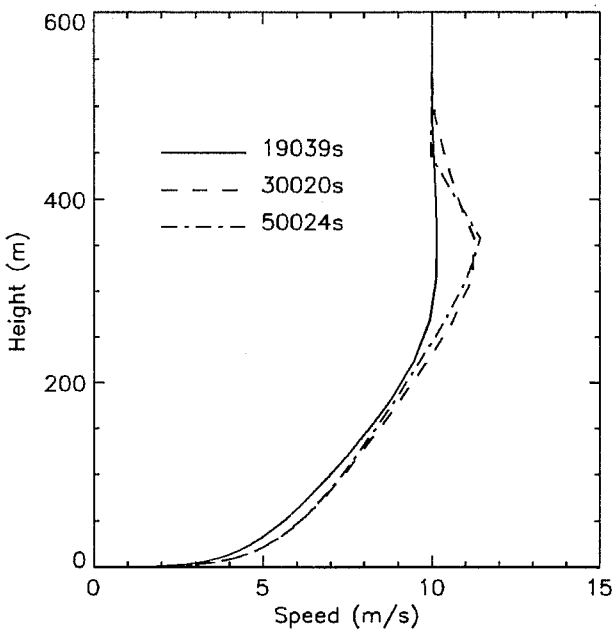

Figure 1: Profiles of wind speed at various times from the stable, one-dimensional, initialization run.

The 300m high hills were grown into the initial profiles, discussed above, over 4000 steps or about 90s simulation time. The simulation was continued for a further 32400s (9 hours) though, as will be shown, a quasi-steady state was achieved after about 7200s or 2 hours. For comparison a neutral simulation of flow over the same hill was made with all the parameters exactly the same as the stable run but with zero surface buoyancy flux. The initial one-dimensional simulation was run for 200000s and results from the two-dimensional case will be shown 100000s after initialization. This simulation is similar to those of Wood and Mason (1993).

2.1 The flow structure

Figure 2 shows streamlines of the flow every 1800s for the first 3 hours of the simulation. In order to show the detail of the flow in the valley a smaller contour interval is used in this region. A contour interval of $25\text{m}^2\text{s}^{-1}$ is used for contours of value greater than $25\text{m}^2\text{s}^{-1}$ and an interval of $2.5\text{m}^2\text{s}^{-1}$ is used for the smaller contour values. Figure 3 is an analogous plot but for the neutral case but only shows the steady state after 100000s of integration. The contour intervals are the same for all the plots in these two figures. At the start of the stable run a deep recirculating separation region is evident in the lee of the hill. This is much deeper and covers a wider section of the valley than that of the

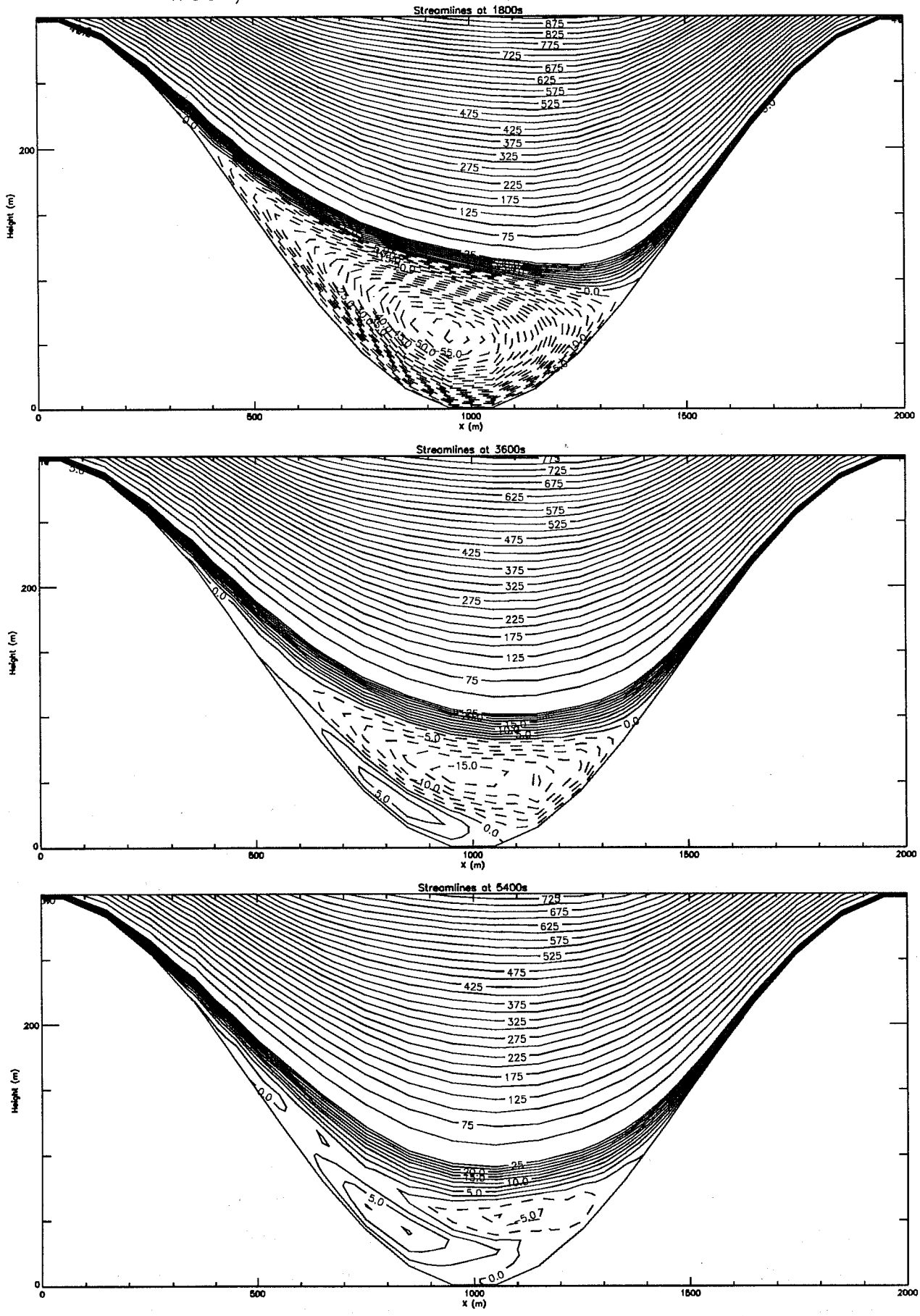

Figure 2: Streamlines from the stable simulation after various times. The contour interval is explained in the text.

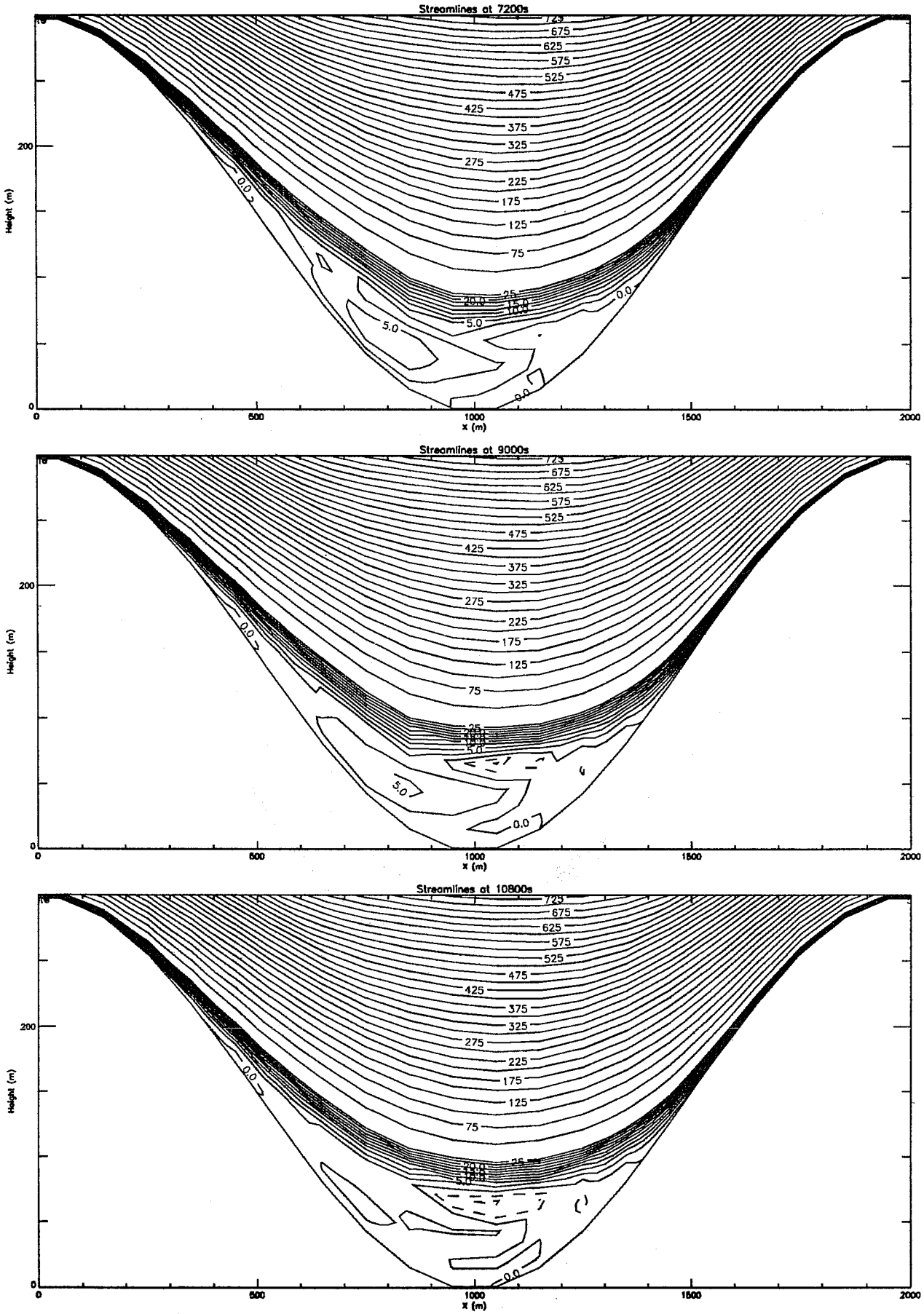

Figure 2: continued

neutral case at any time in its evolution.

As time progresses (3600s and 5400s) it is apparent that the winds on the lee slope of the hill are too weak to overcome a tendency for a drainage current to form. Price (1995) predicts that at this slope and with the imposed buoyancy flux used here then for a slope length of 400m the critical opposing wind speed below which drainage currents may form is approximately 2.5ms^{-1}. At 1800s the upslope wind speed on the lee slope is around 3.0ms^{-1} within the layer where drainage flows subsequently develop. This suggests that either the strength of the recirculation weakens in time or that the situation is just about critical for the formation of drainage currents. Such drainage currents were also found in the simulations of Mason (1987) and the observations of Holden (1998). It is not clear whether a similar effect occurs on the downwind slope as here the sense of the drainage current would be to reinforce the existing downslope flow. However, it does appear that the downslope flow on this side is actually weakening with time suggesting that a drainage current does not form there. Also evident is a reduction in the height of the recirculating region after 5400s to little more than half its original depth and is comparable with the depth of the steady state neutral separation region.

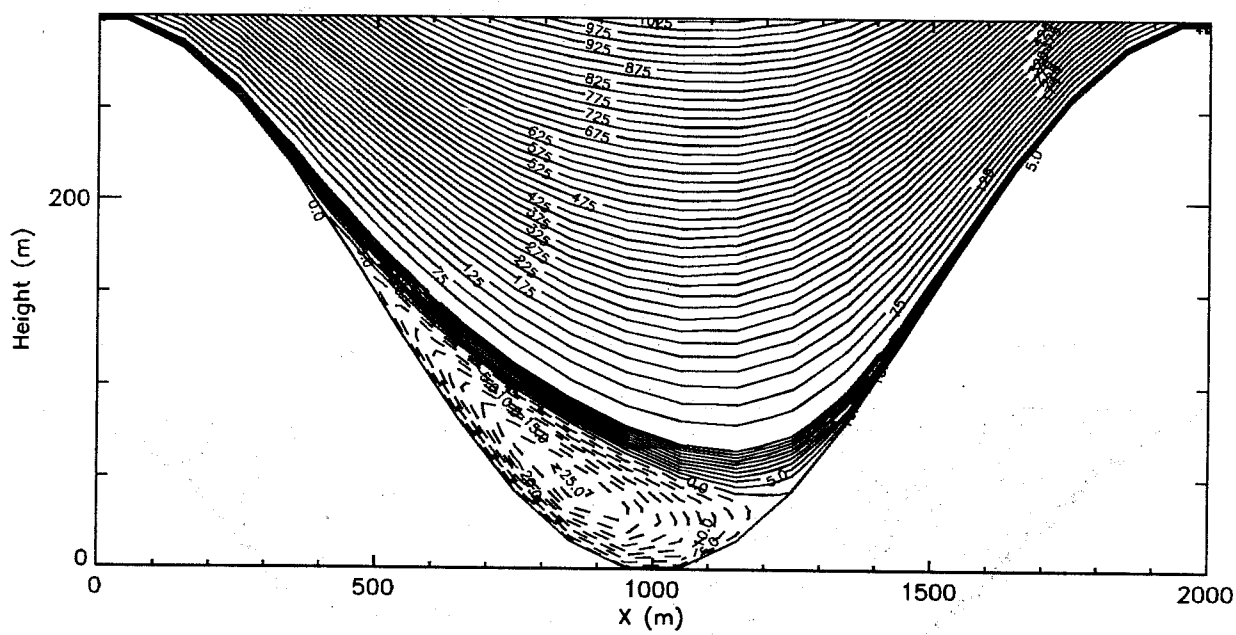

Figure 3: Streamlines from the neutral simulation after 100200s. The contour interval is the same as used in Figure 2 and is explained in the text.

After 5400s, whilst there is quite a clear distinction between the flow near the surface in the valley and the flow aloft, there is no longer a recirculating region. It seems as though the flow in the valley has become very stable, has weakened and become dominated by the drainage flow. As noted by Mason (1987) such drainage currents are poorly modelled in a two-dimensional model valley as there is nowhere for the flow to escape to. Thus the cooled drainage air pools in the valley leading to

strong gradients of temperature and weak shear promoting layers of supercritical Richardson number. Turbulent mixing across these layers is therefore very weak or non-existent leading to the "cut-off" or "decoupled" behaviour observed. Figure 4 shows contours of the buoyancy field (after 21600s), which is linearly related to the potential temperature field. The pooling of cold air in the valley can be seen, in contrast to the slope following contours in the region of the crest. Contours of the gradient Richardson number are shown in Figure 5. Values of Richardson number less than the critical value of 0.33 are contoured with dashed lines. The layers of supercritical Richardson number (solid contours) can be seen in the valley. There is also a larger and more uniform supercritical region above the crest. This will be discussed below.

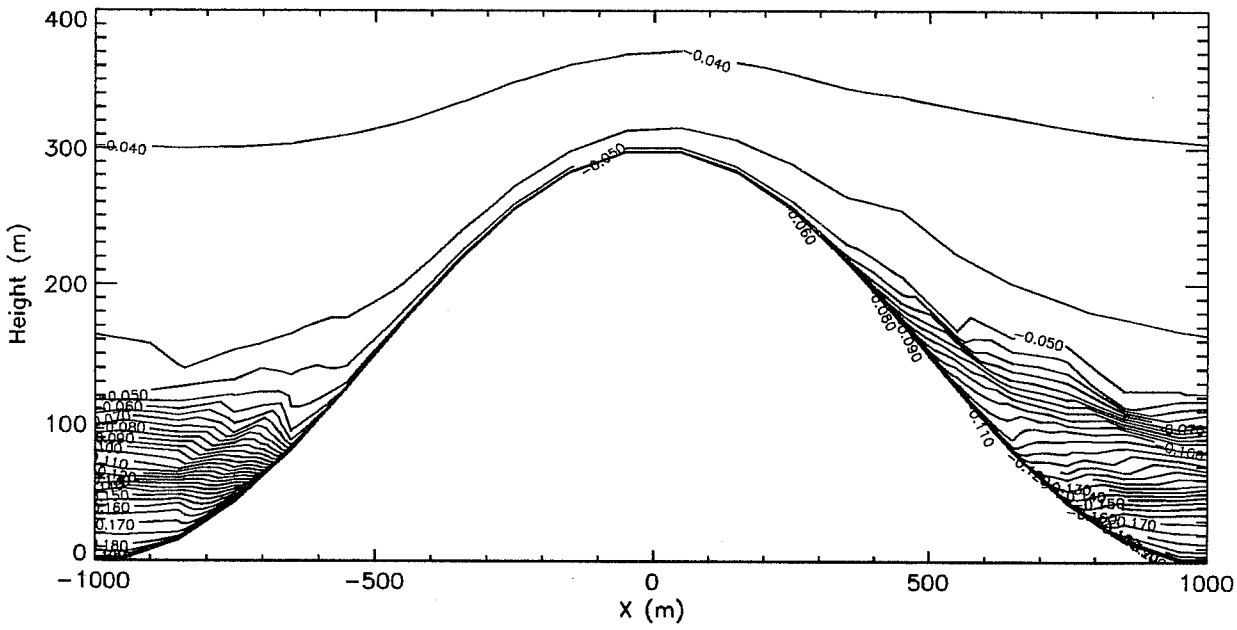

Figure 4: Contours of the buoyancy field from the stable simulation after 21600s. The contour interval is -5×10^{-3}ms^{-2}.

Mason (1987) defined a Froude number as the ratio of the kinetic energy of an air parcel near the crest of the hill to the potential energy needed to lift a parcel of air from the valley bottom to the crest. This number decreases from 2.8 at 1800s to 1.6 after 5400s and reaches a value of 1.3 at 9000s after which it remains constant at this value. This indicates the steadiness of the simulation after the first two hours or so. Also it shows that for this case the dynamic influence of buoyancy is important but not the dominant process. Mason (1987) predicts a resonance between gravity wave type flow modes and the orographic forcing when $U/N \simeq \lambda/2\pi$. Using the above value of F_r and assuming spatial constancy of N this would occur in the present case for a slightly longer hill wavelength of 2450m, assuming that the velocity and buoyancy frequency scales would remain unchanged. It would be interesting to see if this is the case or whether, in view of Mason's similar findings, the flow adjusts and does not admit this resonant motion.

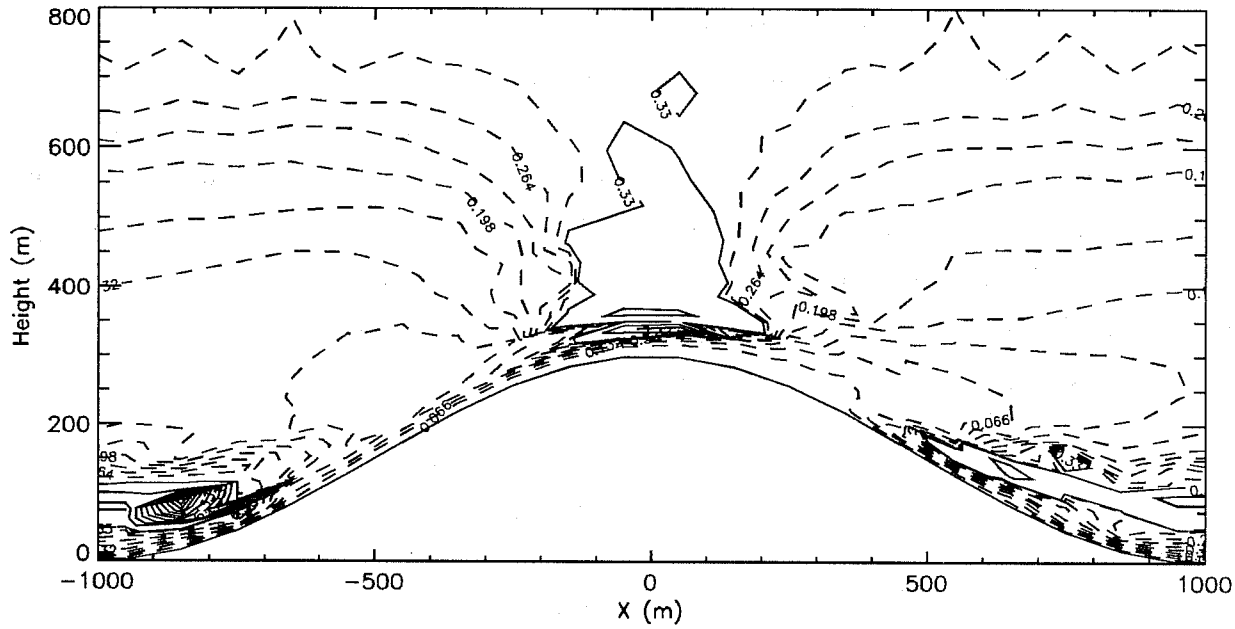

Figure 5: Contours of the gradient Richardson number from the stable simulation after 21600s. The dashed contours are for values less than the critical value of 0.33 and have a contour interval of 0.033. The solid ones are for supercritical values and have a contour interval of 1.

The fractional speed-up of the flow, ΔS, is a useful diagnostic as it characterises some of the changes occurring to the flow. As shown by Hunt *et al.* (1988a), ΔS arises due to the action of both inviscid processes and turbulent processes. It is primarily influenced by shear in the flow, the larger the shear the larger ΔS. In stable conditions the fractional speed-up is therefore expected to increase compared with neutral conditions and Bradley (1983), Frank *et al.* (1993) and Coppin *et al.* (1994) have all observed increases of up to a factor of 2 in ΔS for the most stable cases. In neutral conditions the maximum flow speed-up occurs close to the surface near to but slightly upstream of the crest. In the present simulations as well as those of Belcher and Wood this was still found to be the case.

Using the initial profile of speed as a reference, the neutral simulation discussed above has $\Delta S_{\max} \simeq 0.56$ whilst for the stable case $\Delta S_{\max} \simeq 0.85$. This difference is broadly consistent with the different upstream profiles. Evaluating the fractional speed-up using an average wind speed calculated following the surface of the hill $\Delta S_{\max}$ becomes 0.72 for the neutral run and 0.73 for the stable one. This suggests that there is a marked asymmetry in the neutral flow due to the separation region whereas in the stable case the asymmetry is smaller and it is the flow speed at the crest that dominates the average value.

Having shown the general flow structure we now move to the turbulent aspects. Figure 6 shows contours of the turbulent kinetic energy (TKE) after 21600s. Overlain as shaded areas are regions of supercritical Richardson number. In the shaded regions and just downstream of them there is a marked reduction in TKE whilst there is an elevated maximum of TKE in the valley. This increase

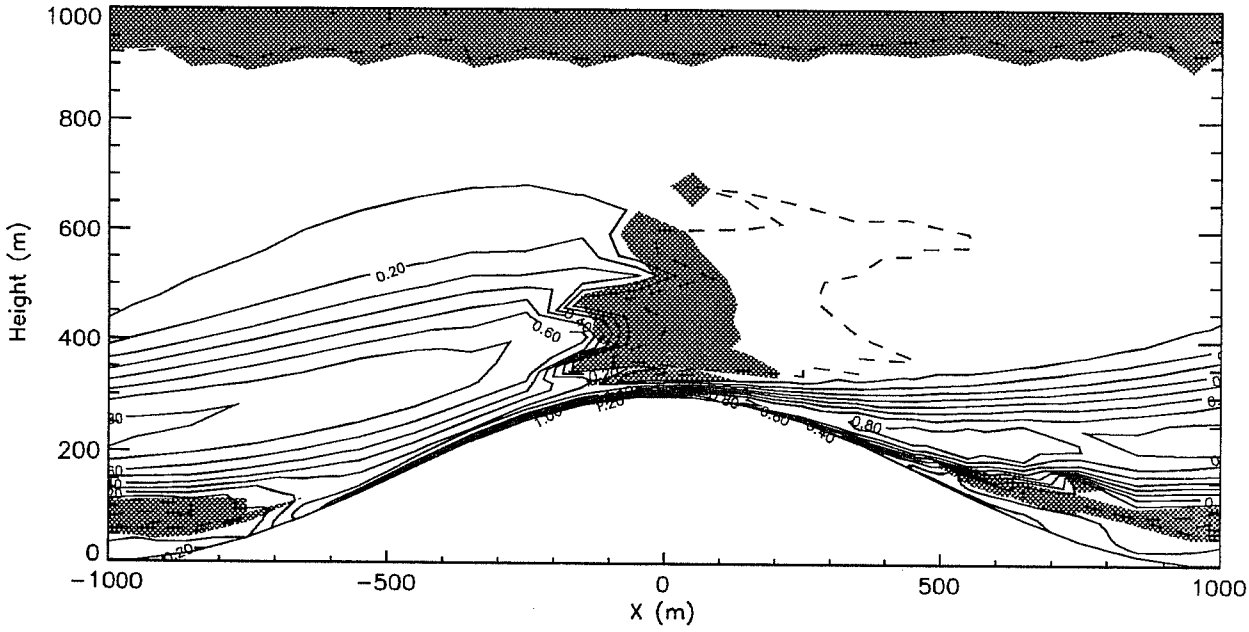

Figure 6: Contours of TKE from the stable run after 21600s. The solid contours have a contour interval of $0.1\mathrm{m}^2\mathrm{s}^{-2}$. The dashed contour has a value of $10^{-3}\mathrm{m}^2\mathrm{s}^{-2}$ and the shaded areas are regions of supercritical Richardson number.

is associated with large vertical shear in the flow above the "cut-off" region discussed above and also with the increase in wind-speed just above the surface at the crest. This shear is due to the no-slip condition imposed at the surface. However, away from the surface the speed increase "fills" in the shear that there would be in the undisturbed flow and significantly reduces the vertical shear. This reduction in shear can be seen in the vertical profile of speed at the crest (Figure 7) compared with the initial wind speed. This reduction in shear leads to a large increase in the Richardson number and hence to a destruction of turbulence above the crest. The contour plot of TKE indicates however that this is a local process embedded within the boundary layer. Above, and 200m or so downstream of this supercritical region the TKE remains positive and continuous though rather weak. This suggests that, despite the "hole", the boundary-layer depth is not dramatically affected locally by the hill. The dashed contour is the $0.001\mathrm{m}^2\mathrm{s}^{-2}$ contour and this appears to give a plausible indication of the behaviour of the boundary-layer depth.

Whilst space precludes inclusion of the figures, profiles of various quantities in the valley have been considered and compared qualitatively with the data of Holden (1998). Though no real attempt was made at matching the actual conditions, the model does capture many of the observed aspects of the flow. For example, in both the field data and model data a low level maximum in wind speed was observed followed by a minimum before the wind increased again above the height of the crest. Very small values of TKE were found near the surface of the valley whilst a large maximum exists at about

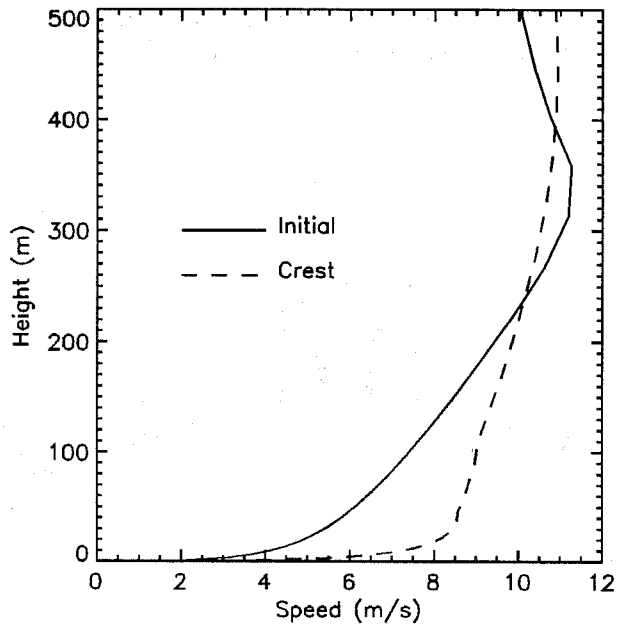

Figure 7: Profiles of wind speed from the stable run. The solid line is the initial profile and the dashed line is the profile above the crest after 21600s.

two thirds of the hill height, just below the height where maximum values of the vertical turbulent momentum and temperature fluxes were found. This level of qualitative agreement suggests that the various simplifications of the simulation were not critical to obtaining reasonably realistic profiles. For example, in contrast to Mason (1987), there is no incoming radiation in the present model and so no differential shading of the sides of the valleys can occur. Also both zero vertical wind shear and zero vertical potential temperature gradient were assumed above the boundary layer.

2.2 Bulk properties of the simulation

We now consider averaged or bulk properties of the simulation.

In terms of parametrizing the influence of the hills on the transfer of momentum the two most important parameters are the total surface drag and the depth of the boundary layer as it is these two parameters that determine the net momentum flux divergence across the boundary layer and hence the net deceleration that the hills exert on the atmosphere. For the one-dimensional simulations the profile of the magnitude of the shear stress can be used to diagnose boundary-layer depth. The height at which the stress has reduced to 5% of its surface value corresponds well with the Zilitinkevich (1972) formula for the boundary-layer depth in stable conditions, Z_i:

$$Z_i \simeq C\sqrt{u_* L_{mo}/f_{\rm cor}} \tag{1}$$

with C taken to be 0.4. u_* is the surface friction velocity and $f_{\rm cor}$ is the Coriolis parameter. From the model results area-averaged (true horizontal averages, relative to gravity) profiles above the height of the crest can be evaluated. Such a profile of stress is shown in Figure 8. Considering the complex processes occurring in the boundary-layer the profile varies reasonably smoothly. From observations of the stress profile Grant and Mason (1990) estimated the "surface" value of stress by extrapolating the profile to the mean height of the orography (here 150m above the valley floor). Such a height is close to the displacement height, at least for neutral flows (Newley 1985; Wood and Mason 1993). Grant and Mason found that the extrapolated surface stress was in good agreement with numerical model estimates of the total surface drag exerted by the orography (the sum of shear stress and pressure force). From the model results this estimate of the surface stress can be evaluated and it has been plotted on Figure 8 at a height of 150m. Clearly this result is not inconsistent with the average stress profile. However any such extrapolation is rather subjective as it depends quite critically on how much importance is attached to the shape of the profile near to the height of the crest.

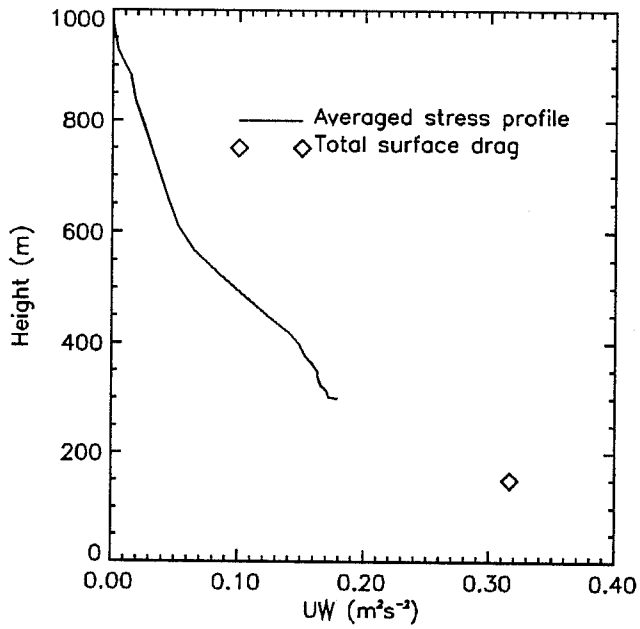

Figure 8: Profile of the total momentum flux. The diamond represents the total surface drag and is plotted at the mean orographic height of 150m.

Here furnished with an independent estimate of the "surface" stress an estimate of the boundary-layer depth can be estimated as the height at which the area-averaged stress has decreased to 5% of its surface value. This gives $Z_i \simeq 875$m above the valley floor. Using the surface stress value discussed above and the imposed surface temperature flux Zilitinkevich's formula (Eq. 1) can be used to estimate Z_i as 870m. The immediate conclusion is that the height of the boundary-layer is therefore in good agreement with what would be expected from a homogeneous boundary-layer with the same surface momentum flux and temperature flux, that is with the same Monin-Obukhov length. However this

neglects the displacement height. Relative to this the boundary-layer height is only 725m. Such a difference in the boundary-layer depth would lead to a 20% change in the modelled stress divergence across the boundary-layer.

We now discuss the total surface drag that was used in the above arguments. The surface drag consists of two components: the averaged surface shear stress and the pressure drag (Wood and Mason (1993) give explicit formulae for these two quantities). The surface shear stresses are quite similar between the two simulations. The pressure drag causes a reduction in the across-ridge flow and the geostrophic balance is broken so that the flow accelerates along the line of the ridges. This leads to an increase in the shear stress in that direction. In the neutral case the total shear stress is reduced from its initial undisturbed value, as is usual for this type of simulation. This is basically because the flow reduction in the lee of the hill outweighs the increase in the flow speed-up at the crest at large slopes (Wood 1992). In the stable case the opposite is found and the total stress is larger than its initial value. Profiles across the hill of the surface stress show that this is due to large increases around the crest and also to some extent down the upstream and downstream slopes. The increase at the crest is due to the large increase in near surface wind speed there compared with the neutral case whilst the increase on the slopes may be due to the presence of drainage currents.

The pressure force is reduced in the stable case by a factor of about 2 compared with the neutral. It is also much more noisy than the neutral one and this, it is believed, is due to the increasing stabilisation of the boundary-layer so that perturbations in the flow are not as effectively damped as in the neutral case. This may be an indication of a weak resolution dependence of the simulation. Linear analysis for this flow configuration (Belcher and Wood 1996) predicts an increase in the pressure drag compared with the neutral case when it is normalised by the undisturbed surface stress and the square of the maximum slope of the hill. Normalising the present pressure drags in this way still indicates a decrease compared with neutral, from 9.8 to 7.0. The analysis of Belcher and Wood shows that the predicted increase is due primarily to the increase in shear of the undisturbed wind speed between the inner-layer height and the middle-layer. It is the fourth power of this shear that enters the analysis. This effect is offset by a reduction in the pressure drag due to the dynamic influence of buoyancy through a multiplicative factor of $(1 - F_L^{-2})$ where F_L is the Froude number of the flow based on the wavelength of the orography. However, for non-linear slopes such as that modelled here there is only limited relevance of the undisturbed flow to the dynamics of the flow since the flow "forgets" its initial value. It is the area-averaged wind profiles that are of more relevance (Wood and Mason 1993) both to the shear and also to the normalising velocity. Figure 9 shows the initial and area-averaged wind speed profiles for both the stable and the neutral cases. It is clear that the area-averaged stable profile is very different from its initial shape and much of the shear in the profile is lost. Near the height of the crest this is presumably largely because of the relatively large flow speed-up occurring

over the crest. The large increase in total surface momentum flux also increases the Monin-Obukhov length from its initial value of 226m to an effective value of 845m, this effective value being based on the total surface momentum and buoyancy fluxes. Thus the averaged flow would be expected to be more neutrally stratified than the initial profiles would suggest and hence to have less shear. Indeed, the shear in the stable profile over the lowest 100m (above the height of the crest) is remarkably close to that of the neutral run. Thus if the area-averaged wind speed is indeed appropriate to the pressure force then the expected increase in the pressure force due to shear in the profile is practically eradicated. The pressure force would then be predicted to be reduced due to the dynamic effect of buoyancy. For this non-linear case it is supposed that a Froude number based on the area-averaged velocity and buoyancy profiles close to the height of the crest is the relevant number. This value is around 1.5 and so neglecting differences in shear the pressure force would be expected to be reduced by approximately 0.56 which is broadly consistent with the model results.

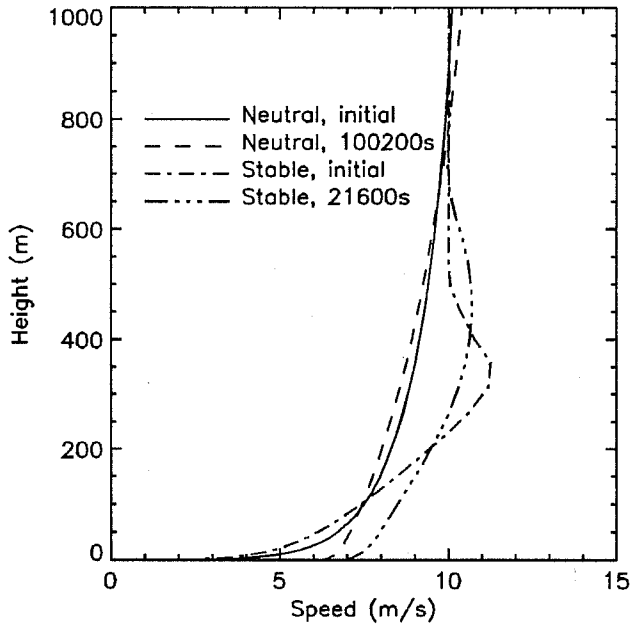

Figure 9: Profiles of the initial wind speed and the area-averaged wind speed for both the neutral (after 100200s) and stable (after 21600s) simulations.

2.3 Parametrization

At this stage it is too early to make any definitive statements regarding methods of parametrizing the drag due to stable, boundary-layer flow over hills. However, in this section some ideas arising from this simulation will be discussed which can be explored in more detail with further simulations in the future. Whilst the thermodynamics of the flow inevitably need to be considered as an integral part of any parametrization of such flows, here we focus only on the total momentum flux.

Perhaps the most pressing question is what should be the form for such a parametrization? For neutral flows it was found that a surface based parametrization was sufficient (i.e. increased surface roughness length) whilst the parametrization of gravity wave drag is currently achieved by specifying the momentum flux profile. The key difference between the two physical processes is that gravity waves induce a large scale vertical momentum flux or alternatively there is a correlation between the ensemble averaged horizontal and vertical velocity fields. This is an inviscid process. In contrast this is not found in neutral flow over hills. The increase in vertical momentum transport is achieved instead by smaller scale, turbulent processes. Further, it is found that such processes do not dramatically change the shape of the area-averaged stress profile, the stress is simply increased in proportion to the increases surface flux. Thus the natural way to parametrize the enhanced momentum flux is only to increase the surface flux via an enhanced roughness length. For stably stratified, turbulent flow over hills it is not clear which or indeed whether both the above mechanisms operates.

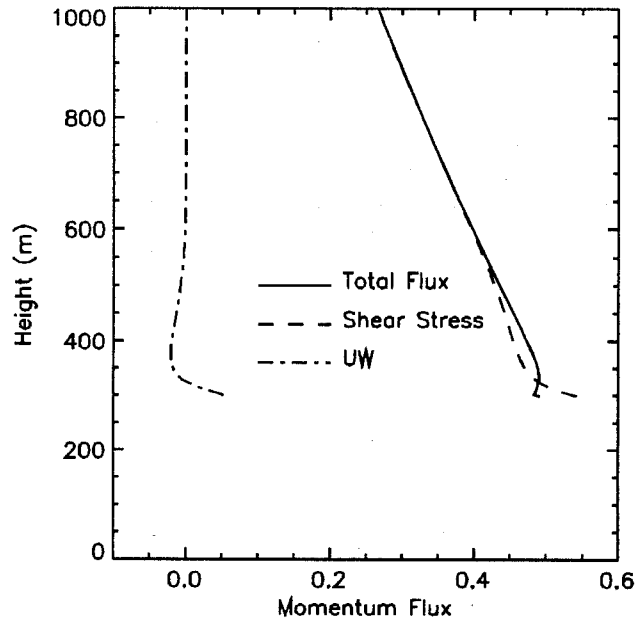

Figure 10: Profiles of the downward turbulent momentum flux (shear stress) and the upward mean flow momentum flux (UW) and together with the total downward flux for the neutral simulation after 100200s.

We can attempt to identify the dominant mechanism by comparing the area-averaged mean momentum flux ($\overline{UW}$) with the area-averaged turbulent negative momentum flux or Reynolds shear stress ($\overline{\tau_{13}}$). Figure 10 shows the vertical profiles of these two quantities together with the total (negative) momentum flux ($\overline{\tau_{13}} - \overline{UW}$) for the neutral case and Figure 11 shows the same profiles for the stable case (the total flux in Figure 11 is what was plotted in Figure 8). It is clear from both figures that the total flux is dominated by the turbulent component of the flux with the mean momentum flux only contributing at all near to the height of the crest of the hill. There is some evidence, though

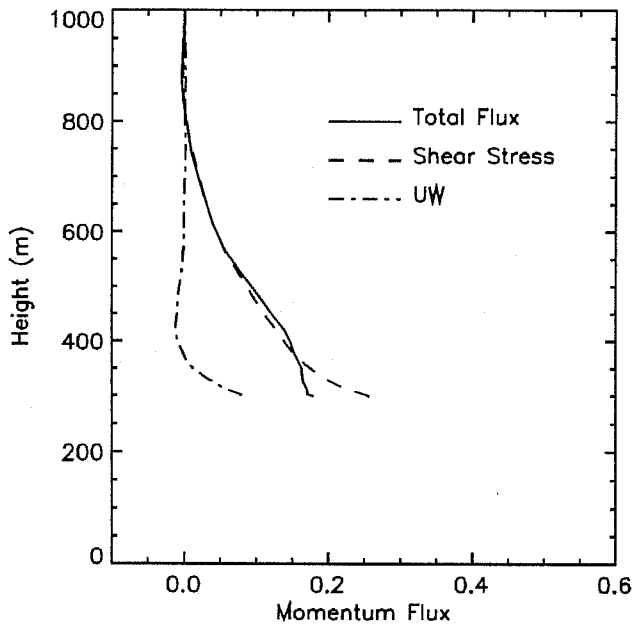

Figure 11: Profiles of the downward turbulent momentum flux (shear stress) and the upward mean flow momentum flux (UW) and together with the total downward flux for the stable simulation after 21600s.

only marginal, that the mean momentum flux is non-zero over a slightly greater depth in the stable case than in the neutral. Based on this simulation alone then it would seem reasonable to seek a parametrization based on the neutral one, though modified to allow for the effects that stability have on the pressure drag discussed above. However, it is anticipated that as the effects of stability increase (either by increased background flow stability or increased wavelength of the hill) then the contribution from the mean momentum flux will increase and it seems likely that a general parametrization will be a combination of both effects. But for the moment that must remain speculation.

Therefore, a parametrization based on an effective roughness length is sought, which in a one-dimensional simulation would give the correct surface stress (denoted here by $u_*^{\text{eff}2}$) and correct boundary-layer depth. To motivate what form of parametrization and what range of appropriate parameters are relevant, the general methodology of Wood and Mason (1993) is followed together with the expression of Belcher and Wood (1996) for the pressure drag modified according to the above discussion.

The basis of the Wood and Mason approach is drag partition which gives:

$$\frac{u_*^{\text{eff}2}}{\overline{U}(Z_m)^2} = \frac{F_p}{\lambda \overline{U}(Z_m)^2} + \frac{{u_{*0}}^2}{\overline{U}(Z_m)^2} \tag{2}$$

where the same assumptions and approximations have been made as in Wood and Mason. Z_m is the pressure height scale which for this simulation, with $h > h_m$, is equal to h. ${u_{*0}}^2$ is the undisturbed

surface stress. F_p is the total pressure force.

From Belcher and Wood (1996) together with the non-linear ideas discussed above F_p is modelled as:

$$\frac{F_p}{\lambda} = \alpha' \left(\frac{\pi A}{S}\right)^2 (1 - F_L^{-2}) \left(\frac{u_{*0}}{U_{hm}}\right)^2 \overline{U}(Z_m)^2 \tag{3}$$

where A is the frontal silhouette area of the hill and S its horizontal surface area so that in this two-dimensional case and for a sinusoidal shaped hill $\pi A/S$ is simply the maximum slope of the hill. F_L is the Froude number at the hill height, which has already been discussed. U_{hm} was used by Wood and Mason (1993) to provide continuity between low slope cases with $h < h_m$ and steeper cases where $h > h_m$. Thus:

$$U_{hm} = \begin{cases} \overline{U}(h_m) & \text{for } h \leq h_m \\ U_{hm} \text{ at } h = h_m & \text{for } h > h_m \end{cases}.$$

α' is a pressure drag coefficient. For presentation purposes here the $(1 - F_L^{-2})$ has been removed from α', so that for low slopes it is related to the pressure drag coefficient of Belcher and Wood (1996), α, by:

$$\alpha' = \alpha(1 - F_L^{-2})^{-1}. \tag{4}$$

We suppose that $\overline{U}(Z)$ has the usual stable, surface-layer similarity form but, as a well as admitting a different roughness length the possibility that the stability function, $\psi_m(Z/L_M)$, is different to the flat case has to be considered. This will be denoted as ψ^{eff}. It is therefore assumed that:

$$\overline{U}(Z_m) = \frac{u_*^{\text{eff}}}{\kappa} \left(\log\left(\frac{Z_m}{Z_{0m}^{\text{eff}}}\right) - \psi_m^{\text{eff}}\right) \tag{5}$$

whilst, following Wood and Mason, u_{*0} is related to $\overline{U}(Z_m)$ by:

$$\overline{U}(Z_m) = \frac{u_{*0}}{\kappa} \left(\log\left(\frac{Z_m}{Z_{0m}}\right) - \psi_m\right). \tag{6}$$

Combining Eqs. 2, 3, 5 and 6 it can be shown that:

$$\log\left(\frac{Z_m}{Z_{0m}^{\text{eff}}}\right) - \psi_m^{\text{eff}} = \left(\log\left(\frac{Z_m}{Z_{0m}}\right) - \psi_m\right) \left(1 + \alpha'(\pi A/S)^2(1 - F_L^{-2})\right)^{-1/2}. \tag{7}$$

Here following the discussion above regarding the pressure force for non-linear slopes α' is simply taken as being approximately equal to its neutral value.

To proceed further use is made of the parametrization for the neutral effective roughness length which will be denoted by Z_{0n}^{eff}. This parametrization is (Wood and Mason 1993):

$$\log\left(\frac{Z_m}{Z_{0n}^{\text{eff}}}\right) = \log\left(\frac{Z_m}{Z_{0m}}\right) \left(1 + \alpha'(\pi A/S)^2\right)^{-1/2}. \tag{8}$$

Equation 8 in Eq. 7 leads to:

$$\log\left(\frac{Z_m}{Z_{0m}^{\text{eff}}}\right) - \psi_m^{\text{eff}} = \log\left(\frac{Z_m}{Z_{0n}^{\text{eff}}}\right)\left(1+\alpha'(\pi A/S)^2\right)^{1/2}\left(1+\alpha'(\pi A/S)^2(1-F_L^{-2})\right)^{-1/2} - \psi_m\left(1+\alpha'(\pi A/S)^2(1-F_L^{-2})\right)^{-1/2}. \quad (9)$$

With no further constraints, this simply gives a relationship between Z_{0m}^{eff} and $\psi_m^{\text{eff}}(Z_m/L_{mo})$, neither being determined uniquely. However, its general form would naturally suggest the following:

$$\log\left(\frac{Z_m}{Z_{0m}^{\text{eff}}}\right) = \log\left(\frac{Z_m}{Z_{0n}^{\text{eff}}}\right)\left(1+\alpha'(\pi A/S)^2\right)^{1/2}\left(1+\alpha'(\pi A/S)^2(1-F_L^{-2})\right)^{-1/2} \quad (10)$$

and

$$\psi_m^{\text{eff}} = \psi_m\left(1+\alpha'(\pi A/S)^2(1-F_L^{-2})\right)^{-1/2}. \quad (11)$$

A value for Z_{0n}^{eff} of 17m has been obtained by matching the surface stress from one-dimensional neutral simulations with the total surface drag from the comparative neutral run discussed before. Using this value for Z_{0n}^{eff} an estimate for α' of 29 is obtained from Eq. 8. The value used for F_L is 1.5 as given previously. Then Eqs. 10 and 11 suggest the following predictions for Z_{0m}^{eff} and ψ_m^{eff} respectively:

$$Z_{0m}^{\text{eff}} \simeq 7.7 \quad (12)$$

and

$$\psi_m^{\text{eff}} \simeq 0.47\psi_m = -(0.47\alpha_{mo})Z/L_{mo}. \quad (13)$$

Since in the model $\psi_m = -\alpha_{mo}Z/L_{mo}$ the change in ψ_m can be modelled as a change in α_{mo}.

Noting the uncertainty in the estimates of α' and F_L it is worth considering the sensitivity of these numbers to changes in each of these parameters. As α' changes from 25 to 33 the predicted value of Z_{0m}^{eff} changes from 7.9m to 7.6m whilst ψ_m^{eff} changes from $0.44\psi_m$ to $0.49\psi_m$. Changing F_L from 1.5 to 1.3 or 1.7 changes Z_{0m}^{eff} to 4.9m and 9.7m respectively while ψ_m^{eff} changes to $0.52\psi_m$ and $0.44\psi_m$ respectively. The results are therefore more sensitive to uncertainties in F_L than in α'.

Also considered are the other possibilities that either Z_{0m}^{eff} remains fixed at its neutral value and ψ_m^{eff} varies or Z_{0m}^{eff} changes and ψ_m^{eff} remains fixed as $-\alpha_{mo}Z/L_{mo}$. Using the above values for α' and Z_{0n}^{eff} these two alternatives give either:

$$Z_{0m}^{\text{eff}} \simeq 17.0 \quad (14)$$

and

$$\psi_m^{\text{eff}} \simeq 1.2\psi_m = -(1.2\alpha')Z/L_{mo}. \quad (15)$$

or

$$Z_{0m}^{\text{eff}} \simeq 13m \quad (16)$$

and

$$\psi_m^{\text{eff}} \simeq \psi_m. \tag{17}$$

Thus three one-dimensional simulations were performed and, based on these results, one further run was also made. The details by which they differ from the initialization run are given in Table 2. Note that the surface buoyancy flux used is the area-averaged value from the two-dimensional simulation allowing for the increased surface area per unit horizontal area due to the curvature of the hill's surface (see Hewer and Wood (1998) for further discussion of this).

Table 2. ONE-DIMENSIONAL PARAMETRIZATION RUNS.

RUN	Z_{0m} (m)	R_{icrit} ($\equiv 1/\alpha_{mo}$)	Surface buoyancy flux (m^2s^{-3})
A	7.5	0.660	5.265×10^{-0}
B	13.0	0.330	"
C	17.0	0.275	"
D	17.0	0.235	"

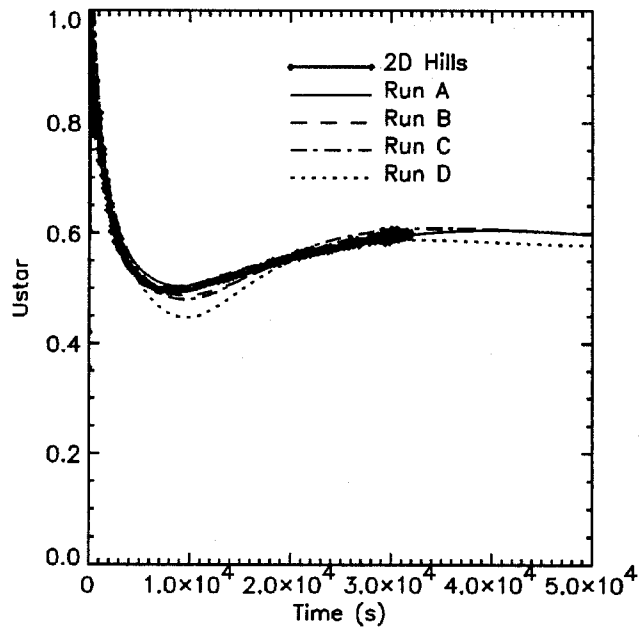

Figure 12: The time series of the effective surface friction velocity (the square root of the total surface drag) for the stable run with the time series of the friction velocities from the one-dimensional runs A, B, C and D.

Figure 12 shows the comparison between the time series of the square root of the total surface drag from the stable two-dimensional run with the friction velocities from the one-dimensional runs. For runs A, B and C there is excellent agreement with the two-dimensional drag values and after about 40000s it is seen that all three simulations have converged to the same value. However, the level of agreement found is to some extent fortuitous as the same limiting length scale in the Blackadar formula has been used as for the initial one-dimensional simulation, namely 100m. Strictly this value should

be modified to allow for changes in the boundary layer depth and this would change the predicted values of u_* slightly. Nevertheless, these results suggest that Eq. 9 is well founded and gives a useful prediction of the relationship between Z_{0m}^{eff} and ψ_m^{eff}.

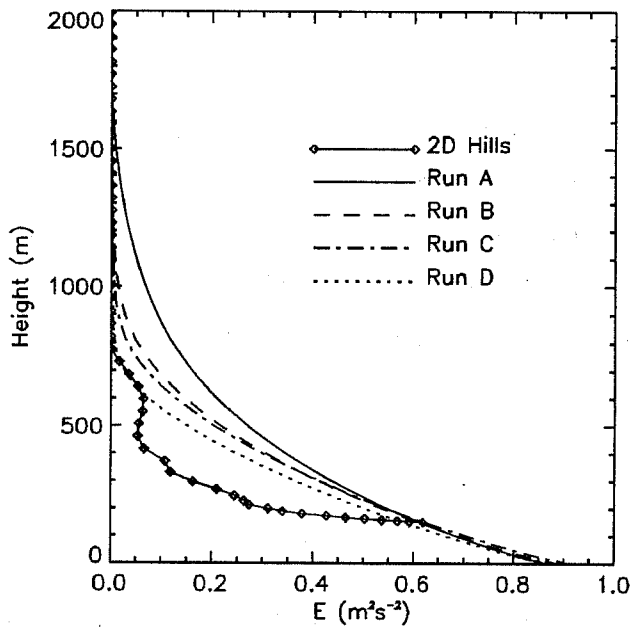

Figure 13: Profile of the area-averaged TKE from the stable run after 21600s, plotted relative to the mean height of the orography, together with TKE profiles at the same time from runs A, B, C and D.

Thus the surface stress of the two-dimensional simulation can be matched in a one-dimensional run. The second parameter that is needed to be well predicted is the boundary-layer depth. In Figure 13 profiles of TKE from the one-dimensional runs are compared with the area-averaged TKE profile from the two-dimensional case, the latter being plotted assuming a displacement height of the mean orographic height, that is 150m. From this figure it is clear that run A has a very deep boundary layer with the depth reducing progressively in runs B and C though even for run C it is still 100-200m deeper than the two-dimensional case.

The boundary-layer depth is related to the critical Richardson number, R_{icrit}, reducing this number reduces the depth. To indicate sensitivity to varying this, run D is the same as run C except the critical Richardson number has been reduced from 0.275 to 0.235. The results from this run are plotted as the dotted lines in Figures 12 and 13. The reduction in R_{icrit} makes the flow more stable and so for fixed surface roughness length the friction velocity is slightly reduced, though the agreement with the two-dimensional run is still very good after an initial settling period of 20000s. The run being more stable though reduces the boundary layer depth thereby achieving excellent agreement with the two-dimensional run. Using the total stress profiles the boundary-layer depth is estimated as 660m. This suggests that, consistent with Eq. 9, the best match to the two-dimensional case, at least as

far as surface stress and boundary-layer depth is concerned, would be achieved with a larger effective surface roughness length of around 21m and an $R_{i\mathrm{crit}}$ of 0.235.

3 DISCUSSION

The above parametrization must be considered highly speculative and its generality requires investigation with further simulations of different flow situations. However, with this caveat it is interesting to consider why it would appear that the effective critical Richardson is reduced in this case. Firstly it is worthwhile distinguishing between what has been referred to so far as the critical Richardson number and what may be considered the real $R_{i\mathrm{crit}}$. The general log-linear stability functions have the form:

$$\phi_m = 1 + \alpha_{mo} Z/L_{mo} \tag{18}$$

and

$$\phi_h = P_r(1 + \beta_{mo} Z/L_{mo}) \tag{19}$$

from which the integrated forms ψ_m and ψ_h follow. Here P_r is the Prandtl number. For such functions the critical Richardson number is $P_r\beta_{mo}/\alpha_{mo}^2$. In the two-dimensional simulation $P_r \equiv 1$ and $\beta_{mo} \equiv \alpha_{mo}$. This is the form that has also been used in all the one-dimensional simulations presented. The averaged thermal structure of the flow has not been considered in detail at all and so it is possible that a more complete parametrization may require P_r to differ from 1 and for β_{mo} to be different from α_{mo}.

Some hints as to the possible behaviour of these other parameters can be found by considering their area-averaged profiles. Using the total momentum and buoyancy fluxes together with the area-averaged profiles of buoyancy and speed a Prandtl number profile from the two-dimensional run can be evaluated. This profile is plotted in Figure 14. There is some variation from its initial value of 1 in that near the height of the crest of the hill it is close to 0.5 whilst aloft it increases to a value between 1.1 and 1.2. However, this variation is small and it is not clear that it is significant. Similarly the area-averaged Richardson number profile can be evaluated from the area-averaged velocity and buoyancy profiles. This is shown in Figure 15. From this there is no compelling evidence to suggest that $R_{i\mathrm{crit}}$ is different from its initial value of 0.33 which is marked as a dashed line. It is possible that it is in fact impossible to match all the relevant properties of the flow simultaneously, e.g. surface momentum flux, boundary-layer depth *and* critical Richardson number. Clearly more work now needs to be done regarding the averaged thermal structure of the flow. However, for the moment it is probably best to interpret the proposed reduction in $R_{i\mathrm{crit}}$ as a reduction in $1/\alpha_{mo}$ attendant on more information regarding the behaviour of β_{mo}.

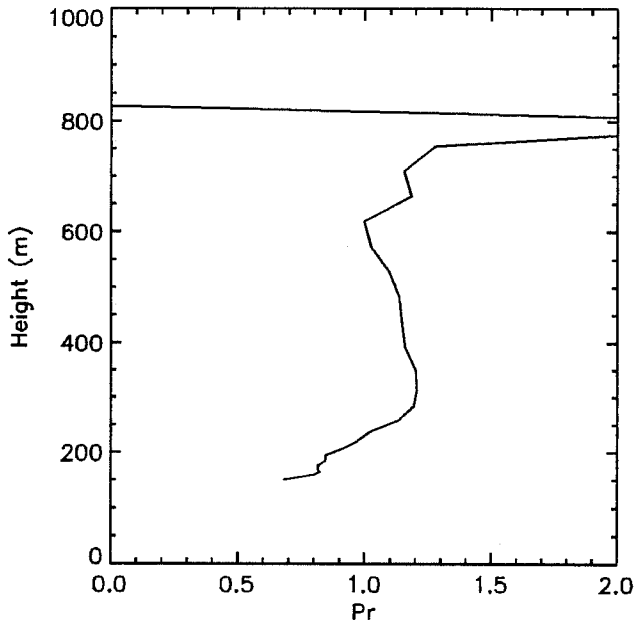

Figure 14: The profile of the Prandtl number from the stable simulation after 21600s. It is evaluated from the area-averaged profiles of velocity, buoyancy, total momentum flux and total buoyancy flux.

Further evidence regarding the values of the stability function constants can be obtained from diagnosed profiles of the stability functions ϕ_m and ϕ_h. These are calculated from surface layer similarity theory as:

$$\phi_m \equiv \frac{\kappa(Z - d + Z_{0m})}{u_*} \left| \frac{\partial \mathbf{U}}{\partial Z} \right| \tag{20}$$

and

$$\phi_h \equiv \frac{\kappa(Z - d + Z_{0m})u_*}{B_*} \frac{\partial B}{\partial Z} \tag{21}$$

where B_* is the surface buoyancy flux. These quantities will not follow exactly the surface layer predictions, that is a linear increase with Z/L_{mo}, since this is only valid in the lowest 10% or so of the boundary layer. But their behaviour relative to different one-dimensional simulations gives some idea of the effective values of α_{mo} and β_{mo}. Figure 16 shows the profiles of ϕ_m and ϕ_h for the two-dimensional run compared with those from runs B and D. In fact the profiles do vary remarkably linearly with normalised height. It is clear that the two-dimensional profiles increase much more quickly with height than the standard profiles of run B suggest. Run D agrees very well with the two-dimensional case for ϕ_m, supporting the use of smaller values of $1/\alpha_{mo}$. The agreement with ϕ_h is much better than for run B but not as good as for ϕ_m. This suggests that an improvement to the suggested parametrization might be achieved by reducing $1/\beta_{mo}$ relative to $1/\alpha_{mo}$ but this must await further investigation of the thermal structure.

So why does the flow seem to produce an average flow with increased α_{mo}? A related question is why does the flow generate such a relatively large vertical flux of momentum but without a com-

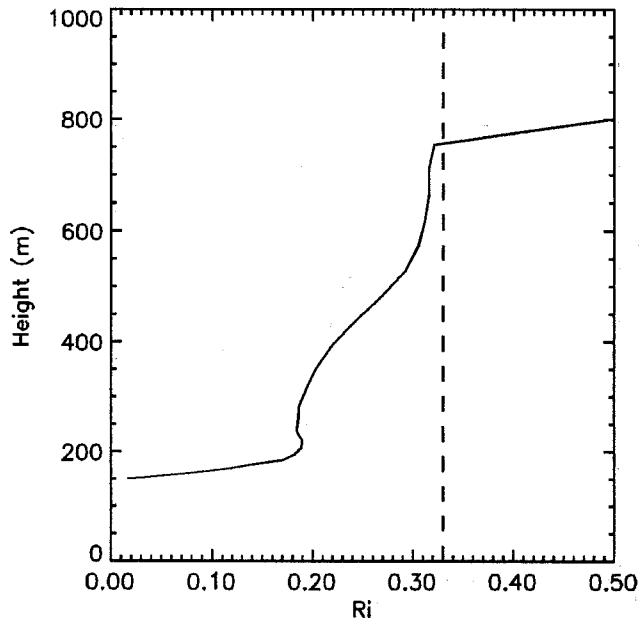

Figure 15: The profile of the gradient Richardson number from the stable simulation after 21600s. It is evaluated from the area-averaged profiles of velocity and buoyancy. The dashed line represents the critical Richardson number used in the turbulence closure of the two-dimensional simulation (0.33).

mensurate growth in the boundary layer? This is evident from comparison of runs A, B and C. The answer seems to lie in the contour plots of TKE and Richardson number presented in Figure 6. Here it was seen that due to the flow speed-up a quite extensive region with super-critical Richardson number forms which is embedded within the boundary layer. This layer will inhibit vertical transfer of momentum, as is evident from the large region of greatly reduced TKE. This reduction in both TKE and Richardson number is evident in the area-averaged profiles of these quantities (Figures 13 and 15). Thus, compared with a flat homogeneous boundary layer with the same surface roughness and buoyancy flux, and hence the same surface momentum flux, the two-dimensional case inhibits the vertical transport of momentum leading to a much shallower boundary layer.

Of course it is not immediately obvious from the contoured values that the average profiles will be so dominated by the super-critical regions near the crest rather than the regions further downstream of the crest where there is large production of TKE. We speculate that for a boundary layer that is initially more stable than the present one, for example one where the initial boundary-layer depth is shallower than the hill height (rather than the same order as the hill height as it is for the present case) then the effects of the hills may be the opposite. It may be then that the increased production of TKE downstream of the crests may dominate the area-averages and we might expect $1/\alpha_{mo}$ to increase.

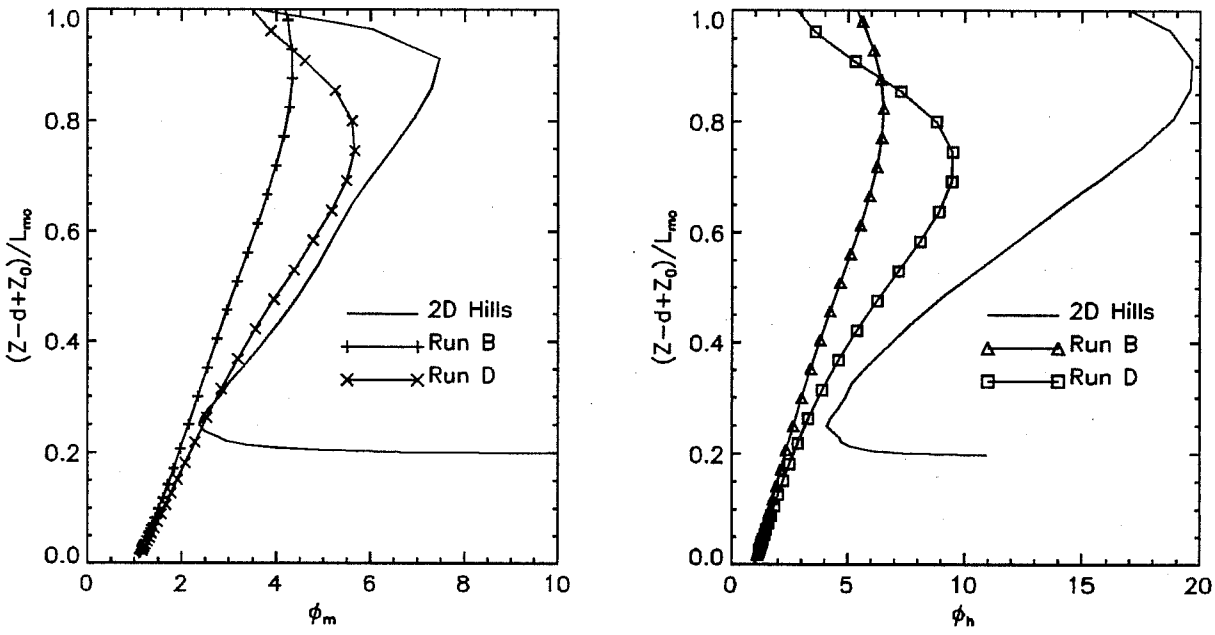

Figure 16: Profiles of the normalised, area-averaged vertical wind shear (ϕ_m) and buoyancy gradient (ϕ_h) plotted against $(Z - d + Z0)/L_{mo}$ for the stable two-dimensional run and the one-dimensional runs B and D. For the stable run a value of 150m has been used for the displacement height, d; L_{mo} equals 845m; and a value of 17m was used for Z_0.

4 CONCLUSIONS

The present study was intended to highlight areas of interest and sensitivity in stable flow over hills with slopes for which linear analysis is not applicable.

A quite complex flow structure has been demonstrated within the valleys with formation of drainage currents coupled with "cut-off" recirculating regions. This leads to generally very weak wind speeds and strong stratification. At the crests large increases in the wind speed associated with increased shear in the undisturbed wind profile leads to enhanced shear near the surface but significantly reduced shear above that. This reduced shear leads to a region of super-critical Richardson number and greatly reduced TKE. In contrast the enhanced shear near the surface of the crest and also above the "cut-off" layer leads to an elevated maximum in TKE downstream of the crest. The boundary-layer depth is approximately double that of the undisturbed boundary-layer though there is evidence that this is still smaller than would be expected for a comparable homogeneous boundary layer with the same net surface momentum flux.

The form of the profiles of horizontally averaged turbulent and mean flow momentum fluxes are reasonably similar to those found in neutral flows. This suggests that a roughness length based

parametrization is appropriate though the possibility of modifications to the stability dependence of the flow must be considered.

The total pressure drag is found to be dominated by the dynamic effect of buoyancy on the flow whilst the kinematic effect due to shear in the flow is significantly reduced from the low slope case and is close to the neutral steep case. An expression relating the effective roughness length for momentum and an effective stability parameter has been given based on general expressions developed by Belcher and Wood (1996) together with the methodology of Wood and Mason (1993). One-dimensional simulations were performed using parameters obtained from this expression in which, for given geostrophic wind, it was attempted to match the surface momentum flux and boundary-layer depth so as to achieve the correct bulk momentum flux divergence. These suggest that the effective roughness length remains close to its neutral value whilst the effective stability of the flow (as represented by α_{mo}) is increased from its flat, homogeneous value.

The generality of these conclusions needs now to be investigated in a variety of situations, such as for varying slope, stability, boundary-layer depth relative to hill height etc. It is hoped that using the ideas proposed here and modifications based on these further simulations a robust parametrization of the important flow features can be developed. Here though we have focussed on the momentum structure and development of a general parametrization will require a detailed study the averaged thermal structure which has not been attempted here. Also, it seems likely that three-dimensional effects may become important especially for the very stable cases.

Acknowledgement

I should like to express my gratitude to Fiona Hewer for her help and many useful discussions during this work.

5 REFERENCES

Belcher, S.E., Newley, T.M.J. and Hunt, J.C.R. 1993 The drag on an undulating surface induced by the flow of a turbulent boundary layer. *J. Fluid Mech.*, **249**, 557–596.

Belcher, S.E. and Wood, N. 1996 Form and wave drag due to stably stratified turbulent flow over low ridges. *Quart. J. Roy. Meteorol. Soc.*, **122**, 863–902.

Bradley, E.F. 1983 The influence of thermal stability and angle of attack on the acceleration of wind up a slope. *J. Wind Eng. and Indust. Aerodyn.*, **15**, 231–242

Caughey, S.J., Wyngaard, J.C. and Kaimal, J.C. 1979 Turbulence in the evolving stable boundary layer. *J. Atmos. Sci.*, **6**, 1041–1052.

Chimonas, G. and Nappo, C.J. 1989 Wave drag in the planetary boundary layer over complex terrain. *Bound. Layer Meteor.*, **47**, 217–232.

Coppin, P.A., Bradley, E.F. and Finnigan, J.J. 1994 Measurements of flow over an elongated ridge and its thermal stability dependence: the mean field. *Bound. Layer Meteor.*, **69**, 173–199.

Derbyshire, S.H. 1995 Stable boundary layers: observations, models and variability part I: modelling and measurements. *Bound. Layer Meteor.*, **74**, 19–54.

Derbyshire, S.H. and Wood, N. 1994 The sensitivity of stable boundary layers to small slopes and other influences. pp.105-138, *Proc. 4th IMA Conf. Waves and Stably-Stratified Turbulence*, ed. N.Rockliff and I.P.Castro. Clarendon Press, Oxford.

Dörnbrack, A. and Schumann, U. 1993 Numerical simulation of turbulent convection flow over wavy terrain. *Bound. Layer Meteor.*, **65**, 323–355.

Frank, H., Heldt, K., Emeis, S. and Fiedler,F. 1993 Flow over an embankment: speed-up and pressure perturbation. *Bound. Layer Meteor.*, **63**, 163–182.

Grant, A.L.M. and Mason P.J. 1990 Observations of boundary layer structure over complex terrain. *Quart. J. Roy. Meteorol. Soc.*, **116**, 159–186.

Grisogono, B. 1994 Dissipation of wave drag in the atmospheric boundary-layer. *J. Atmos. Sci.*, **51**, 1237–1243.

Hewer, F.E. and Wood, N. 1998 The effective roughness length for scalar transfer in neutral conditions over hilly terrain. *Quart. J. Roy. Meteor. Soc.*, (in press)

Holden, J.J. 1998 Stable boundary layer flow over hills. Ph.D. dissertation, Reading University.

Hunt, J.C.R., Leibovich, S. and Richards, K.J. 1988a Turbulent shear flows over low hills. *Quart. J. Roy. Meteorol. Soc.*, **114**, 1435–1470.

Hunt, J.C.R. and Richards, K.J. 1984 Stratified airflow over one or two hills. *Bound. Layer Meteor.*, **30**, 223–259.

Hunt, J.C.R., Richards, K.J. and Brighton, P.W.M. 1988b Stably stratified shear flow over low hills. *Quart. J. Roy. Meteorol. Soc.*, **114**, 859–886.

Inglis, D.W.F., Choularton, T.W., Stromberg, I.M.F., Gardiner, B.A. and Hill, M. 1995 Testing of a linear airflow model for flow over complex terrain and subject to stable, structured stratification. pp. 88-132, *Wind and Trees* Eds. Coutts, M.P. and Grace. J., Cambridge University Press.

Krettenauer, K. and Schumann, U. 1992 Numerical simulation of turbulent convection over wavy terrain. *J. Fluid Mech.*, **237**, 261–299.

Leonard, B.P., MacVean, M.K. and Lock, A.P. 1993 Positivity-preserving numerical schemes for multidimensional advection. NASA Technical Memo. 106055, ICOMP-93-05.

Mahrt, L. 1982 Momentum balance of gravity flows. *J. Atmos. Sci.*, **39**, 2701–2711.

Mason, P.J. 1987 Diurnal variations in flow over a succession of ridges and valleys. *Quart. J. Roy. Meteorol. Soc.*, **113**, 1117–1140.

Newley, T.M.J. 1985 Turbulent airflow over hills. Ph.D. dissertation, Cambridge University

Ólafsson, H. and Bougeault, P. 1997 Why was there no wave breaking in PYREX? *Beitr. Phys. Atmosph.*, **70**, 167-170

Piacsek, S.A. and Williams, G.P. 1970 Conservation properties of convection difference schemes. *J. Comput. Phys.*, **6**, 392-405

Price, J.C.W. 1995 *the influence of ambient winds on atmospheric drainage flows.*, Ph.D. dissertation, Queen Mary and Westfield College, London.

Schumann,U. 1990 Large-eddy simulation of the up-slope boundary layer. *Quart. J. Roy. Meteorol. Soc.*, **116**, 637–670.

Shutts, G., and Broad, A. 1993 A case study of lee waves over the Lake District in northern England. *Quart. J. Roy. Meteorol. Soc.*, **119**, 377–408.

Stromberg, I.M., Mill, C.S., Choularton, T.W. and Gallagher, M.W. 1989 *Bound. Layer Meteor.*, **46**, 153–168.

Weng, W., Chan, L., Taylor, P.A. and Xu, D. 1997 Modelling Stably Stratified Boundary Layer Flow over Low Hills. *Quart. J. Roy. Meteorol. Soc.*, **123**, 1841–1866.

Wood, N. 1992 Turbulent flow over three-dimensional hills. Ph.D. dissertation, Reading University.

Wood, N. and Mason, P.J. 1993 The pressure force induced by neutral, turbulent flow over hills. *Quart. J. Roy. Meteorol. Soc.*, **119**, 1233–1267.

Zhou, J., Taylor, P.A. and Qi,Y. 1995 Dynamic processes in stably stratified boundary layer flows over topography. pp. 462-465. In *Proceedings of the 11^{th} Symposium on Boundary Layers and Turbulence*, Charlotte, N.C. March 1995.

Zilitinkevich, S.S. 1972 On the determination of the height of the Ekman boundary layer. *Bound. Layer Meteor.*, **3**, 141–145.